

Analysis of Plate Bone Construct Failure Following Tibial Tuberosity Advancement

W. T. McCartney^{1,2}

E. Galvin²

B Mac Donald

D Comiskey³

¹Marie Louise Veterinary Hospital, Baldoyle, Dublin 13, Ireland

²MDORC, School of Mechanical & Manufacturing Engineering, Dublin City University, Dublin 9, Ireland

³Bahrain Polytechnic, Isa Town, Kingdom of Bahrain

KEY WORDS: Finite element analysis, FEA, tibial tuberosity advancement, TTA, cranial cruciate ligament, CCL, stifle, canine

ABSTRACT

Tuberosity Advancement (TTA) is an operation to repair cranial cruciate ligament rupture in dogs. A review of previously unsuccessful TTA procedures was undertaken in an attempt to characterise the nature of bone failure. The x-rays demonstrated that failure of the advanced tibial tuberosity normally occurred in the gap between the cage/screw and fork/plate. A finite element model of a tibial tuberosity advancement (TTA) was constructed and three different tension band plate (TBP) placement strategies were examined. In each of the three case studies, the distance between the cage hole and the top hole of the TBP was varied. The finding suggests that the cage hole may be a stress raiser, particularly when the TBP fork is mounted below the level of the cage hole.

INTRODUCTION

Tibial tuberosity advancement (TTA) is an orthopaedic procedure to repair deficient (eg, partially torn/ruptured) cranial cruciate ligaments (CCL) in dogs, and was developed in the late 1990's.¹ The TTA procedure was developed based on biomechanical analysis

of the joint forces of the human knee² and other in vitro studies.^{3,4} The model shows that the tibiofemoral compressive force was the same as the patellar tendon force, which resulted in a variable tibiofemoral shear force that was directed either anterior or posterior dependent upon knee flexion/extension.⁵ The magnitude of the shear force was determined by the patellar tendon angle (PTA).⁵ TTA alters the direction of the patellar tendon force maintaining either a neutral or a caudal directed tibiofemoral shear force during weight bearing.² The TTA was introduced to clinical use in 2004, and some peer-reviewed publications reporting clinical outcomes have been published.^{6,7}

MATERIALS AND METHODS

A review of previously unsuccessful TTA procedures was undertaken in an attempt to characterise the nature of bone failure. The x-rays demonstrated that failure of the advanced tibial tuberosity normally occurred in the gap between the cage/screw and fork/plate. It was hypothesised that the common factor in all these cases was that the top fork was positioned below the point of the quadriceps insertion thus increasing the tensile stress induced in the cranial aspect of the tibia and initiating fracture at this site

Figure 1 Post operative TTA failure case showing tibial tuberosity fracture

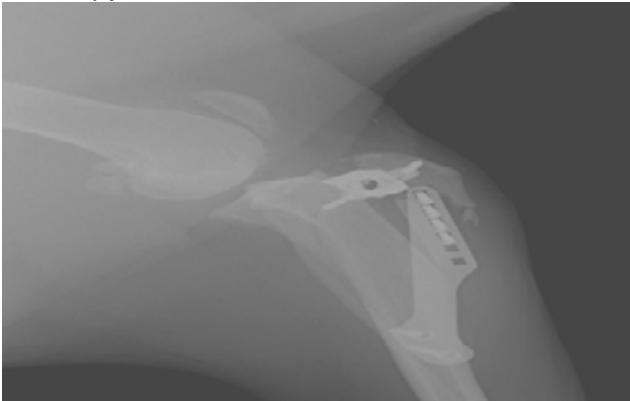


(Figure 1). It was noted that in successful TTA procedures that the distance between the cage screw and top fork insertion point was much smaller than in the unsuccessful cases. Therefore, it was hypothesised that the distance between the quadriceps insertion and first fork was critical to the clinical outcome, and should be minimised. In order to test this hypothesis, three finite element models were developed where the spacing between the cage hole and top fork (in the y-direction) was varied.

A finite element model of a tibial tuberosity advancement (TTA) was constructed and three different tension band plate (TBP) placement strategies were examined. In each of the three case studies, the distance between the cage hole and the top hole of the TBP was varied. In order to generate the simulations pertaining to each case study, the finite element model required a number of inputs, namely: the geometry of the advanced tibial tuberosity, the patellar tendon, and the implants; the material properties of the bone, tendon, and implants; and the appropriate application of loading and boundary conditions, as described later.

The 3-D geometry of the stifle joint was simplified using a 2-D plane strain assumption. In this model, the thickness dimension (z) is assumed to be much larger than the other two dimensions (x,y), the loads and deformations, are assumed

to act in the x-y plane, and the loads are assumed to be constant along the length of the model (z).

A model of the advanced tibial tuberosity was derived from mediolateral x-rays of a TTA performed on a 30 Kg dog. The resulting profile was employed to produce a 2-D plane strain model, as shown in Figures 2Aa and 2B. The patellar tendon was modelled as an idealised rectangular geometry with a thickness of 2 mm (the canine patellar tendon

has an elliptical form with a thickness of approximately 2 mm and width of 6 mm). By using appropriate boundary conditions, it was not necessary to model all of the implant components used in the TTA. The cage and TBP were omitted from the model but the cage screw and the fork were modelled as idealised cylinders. The location of the cage screw was derived from the x-ray. The centre of the six holes of the TBP fork were 5mm apart, the same spacing used on the actual TBP. Three different tension

Figure 2A: Mediolateral x-ray of dog stifle TTA **Figure 2B:** FEA model of advanced tibial tuberosity

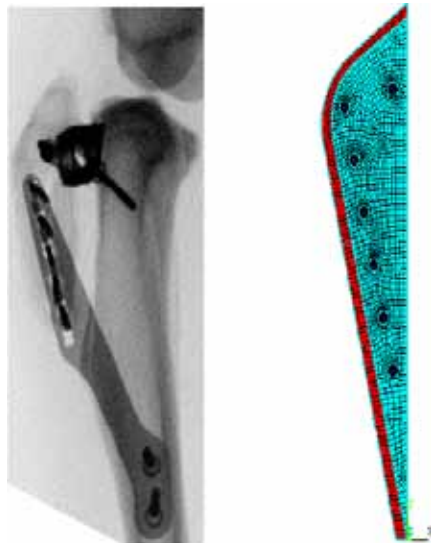
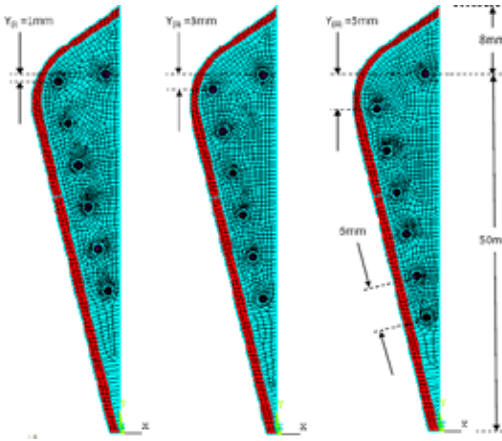


Figure 3: FE models for case study (i), (ii), and (iii). Cage hole and plate hole centres 2mm and 2.5mm from edge of bone, respectively. Diameter of all holes = 1.5mm.



band plate (TBP) placement strategies were examined. In each of the three case studies the distance between the cage hole and the top hole of the TBP fork, in the y-direction, was varied, as illustrated in Figure 3. The distances used were $Y(i)=1\text{mm}$, $Y(ii)=3\text{mm}$, and $Y(iii)=5\text{mm}$, for cases study (i), (ii), and (iii) respectively.

All geometries were meshed with 2-D 8-node plane strain solid elements (Ansys element type Plane183). This element type was selected as it is suitable for modelling deformation of the almost incompressible hyperelastic material of the tendon, using the mixed element formulation. The total number of elements used to mesh the entire model was 4850, chosen based on mesh sensitivity studies. All elements were checked to ensure that no distorted elements were generated and element distortion control was used to prevent inaccuracies arising from excessive distortion of elements in the contact regions.

Material Properties

The material of the bone was modelled using a linear elastic isotropic material model where the Elastic Modulus, $E=1.24\text{GPa}$, and Poisson's ratio, $\nu=0.33$. The material of the screws and fork were modelled using a linear elastic isotropic

material model where $E=200\text{GPa}$ and $\nu=0.3$. The material of the patellar tendon was modelled using a 5-parameter Mooney Rivlin hyperelastic material model. The Mooney Rivlin parameters were derived from uniaxial tensile test data obtained from a previous study involving canine patellar tendon samples,⁸ and had the following values: $C10=1.0732\text{GPa}$, $C01=-1.0351\text{GPa}$, $C20=127.01\text{GPa}$, $C11=-289.09\text{GPa}$, and $C02=164\text{GPa}$. Figure 4 shows the fitted hyperelastic material model obtained in Ansys and the original tensile test data.

Boundary Conditions

The standard 2-D surface-to-surface contact algorithm available in Ansys was used to model the contact between the tibial tuberosity, patellar tendon, TBP fork, and the cage screw, using frictionless contact with the default properties in all models. In addition, the nodes of the cage screw and fork pins was constrained in all degrees of freedom (DOF). Tethering of the patellar tendon to the tibial tuberosity was approximated by constraining all DOF on the end of the patellar tendon. Previous studies suggest that the maximum in vivo strain experienced in the canine patellar tendon corresponds to a strain of approximately 25% and occurs during running.⁹ In

Figure 4: 5-parameter Mooney Rivlin Hyperelastic Material model fitted to experimental engineering stress-strain curve for canine patellar tendon.

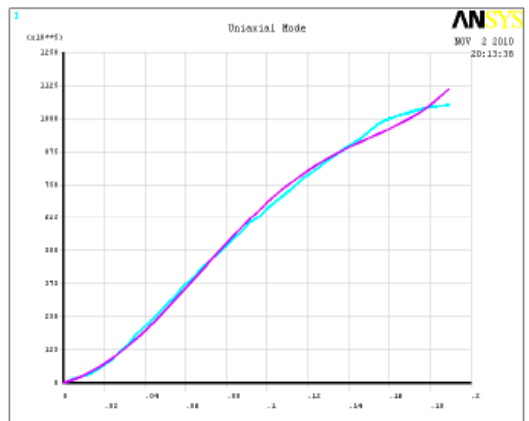
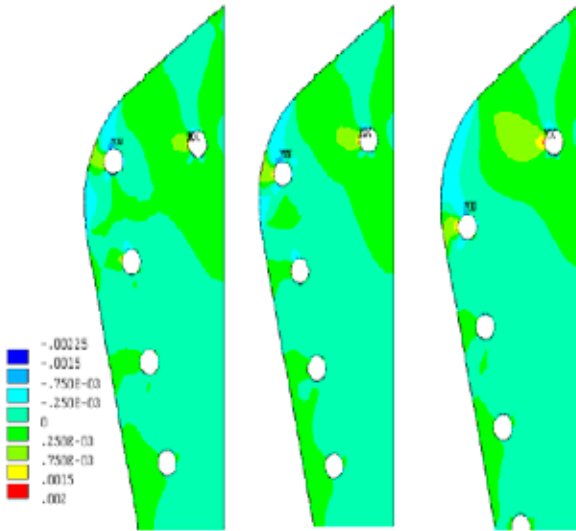


Figure 5: Contour plot of elastic strain in the Y-direction. From left to right: case study (i), (ii) and (iii).



this work, a displacement load of 2.6 mm was applied to the end nodes of the patellar tendon to simulate a strain of 8.5%, corresponding to the approximate patellar tendon strain expected during walking. Each of the three case studies was solved in Ansys using a large-displacement static analysis that employed 100 sub-steps.

RESULTS

The results of the three finite element case studies indicated that the placement of the TBP had a significant impact on the distribution of stresses and strains in the advanced tibial tuberosity. It is well known that bone can support greater loads in compression than bone in tension. Hence, the elastic strain in the y-direction was examined for each model, where positive elastic strain indicated tensile loading. It was noted that significantly greater tension was observed in the cranial aspect of the tibia for case study (ii) and (iii), compared to case study (i). This is illustrated in Figure 5 where there are higher levels of elastic strain in the y-direction. Similarly, the maximum elastic strain level in the y-direction was significantly larger for case study

(ii) and (iii), compared to case study (i). As Table 1 shows, the maximum elastic strain in the y-direction was 0.00093, 0.00117, and 0.00174 for case study (i), (ii), and (iii), respectively.

As Figure 6 demonstrates, there is a more even distribution of stress, and indeed lower levels of stress, in the cranial aspect of the tibia for case study (i), compared to case study (ii) and (iii). In case study (ii) and (iii), VonMises stress levels are significantly higher around the cage hole and the top hole of the TBP fork.

DISCUSSION

It is well known that bone can support greater loads in compression than bone in tension. A review of clinical TTA failure cases

indicated that failure of the bone was more common in the cranial portion of the tibial tuberosity. Further, failure in this region was more common when the top hole of the TBP fork was placed below the level of the cage screw. This finding was supported by the results of the FE studies where elastic strain levels in the y-direction were significantly greater for case study (ii) and (iii) when the fork/cage hole spacing was greatest. In the

Figure 6: Contour plot of VonMises stress. From left to right: case study (i), (ii) and (iii).

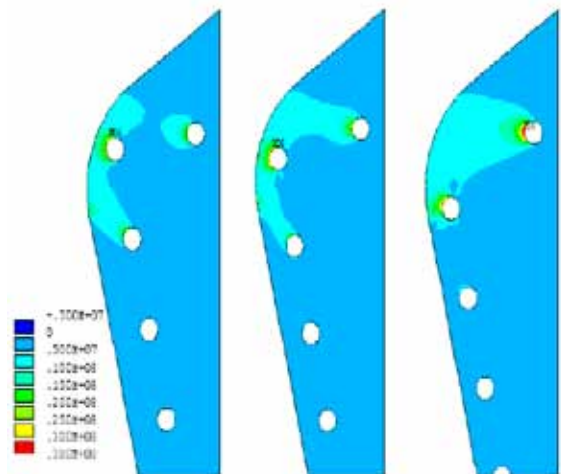


Table 1: Minimum and maximum values of strain in the x and y direction and hydrostatic pressure for case study (i), (ii), and (iii).

	Case study (i)	Case study (ii)	Case study (iii)
Y-Strain _{min}	-0.00132	-0.00143	-0.00115
Y-Strain _{max}	0.00093	0.00117	0.00174
X-Strain _{min}	-0.00175	-0.00179	-0.0025
X-Strain _{max}	0.001	0.0012	0.001
Hydrostatic Pressure _{min} (MPa)	-7.51	-7.71	-6.21
Hydrostatic Pressure _{max} (MPa)	2.29	3.31	3.12
VonMises stress (MPa)	2.59	2.78	3.74

clinical review, it was noted that in many of the cases involving failure, the line of failure passed through the hole that was drilled for the cage screw. Again, the Von Mises stress results from the FE studies supported this finding, where significantly higher stresses were noted around the cage hole for cases study (ii) and (iii), compared to case study (i). This finding suggests that the cage hole may be a stress raiser, particularly when the TBP fork is mounted below the level of the cage hole.

As Figure 6 demonstrates, there is a more even distribution of stress amongst the pins of the forks and the cage hole, and lower stress levels around each of the holes, for case study (i), whereas for case study (ii) and (iii), Von Mises stress is concentrated around the cage hole and the top hole of the fork, where significantly greater stress levels can be observed. Of the three TBP placement strategies simulated in this work, it appears that case study (i) provides the best solution as it results in a more even distribution of loading amongst the pins of the TBP fork and the cage screw, and a significant reduction in the maximum Von Mises stress and maximum elastic strain in the y-direction, observed in the bone material.

CONCLUSION

When using the technique of tibial tuberosity transposition the distance between the top of the fork and the cranial screw of the

cage should be kept to a minimum.

REFERENCES

- Schmoedel H, Montavon P. Versetzung der tuberositas tibiae mit einer kranialisation bei der patellaluxation beim hund. *Kleintierpraxis* 1993;38:805-808.
- Tepic S, Damur D, Montavon P. Biomechanics of the stifle joint, *Proceeding 1st World Orthopaedic Veterinary Congress ESVOT-VOS*, Munich, Germany, 2002; pp 189-190.
- Kipfer N, Tepic S, Damur D, et al. Effect of tibial tuberosity advancement on femorotibial shear in cranial cruciate-deficient stifles. An in vitro study. *Vet Comp Orthop Traumatol* 2008;21:385-390.
- Apelt D, Kowleski MP & Boudrieu RB. Effect of tibial tuberosity advancement on cranial tibial subluxation in canine cranial cruciate deficient stifle joints:an In vitro experimental study. *Vet Surgery* 2007; 36:170-177.
- Nisell R, Ekholm J. Joint load during the parallel squat in powerlifting and force analysis of in vivo bilateral quadriceps tendon rupture. *Scand J Sp Sci* 1986;8, 63-70.
- Hoffman DE, Miller JM, Lanz OI, Martin RA, Shires PK. Tibial tuberosity advancement in 65 canine stifles. *Vet Comp OrthopTraumatol* 2006;19 (4), 219-227.
- Lafaver S, Miller NA, Stubbs WP, Taylor RA & Boudrieu RB. Tibial tuberosity advancement for stabilisation of the cranial cruciate ligament deficient stifle joint: surgical technique, early results and complications in 101 dogs. *Vet Surgery* 2007; 36, 573-586.
- Munns SW, Jayaraman G, Lualin SR. Effect of pretwist on biomechanical properties of canine patella tendon. *J Athros Rel Surg* 1994 ;10, 4, 404-411.
- Ballagas AJ, Montgomery RD, Henderson RA, Gillette R. Pre and post operative force plate analysis of dogs with experimentally transected cranial cruciate ligaments using tibial plateau levelling osteotomy. *Vet Surgery* 2004;333:187-190.